

Figure S1 Skeletal muscle-specific *Bmal1* knockout mice

(A) Scheme showing the generation of muscle-specific *Bmal1* knockout (mKO) mice. The exon encoding the BMAL1 basic helix-loop-helix DNA binding domain (open box) is deleted by Cre recombinase under control of the myosin light chain 1f (*Mlc1f*) promoter. (B) PCR products amplified from mouse DNA demonstrating the conditional floxed *Bmal1* allele (0.43kb band) in tissues from control mice (*Bmal1*^{f/f}; *Mlc1f-Cre*^{-/-}) and disruption of the *Bmal1* gene (excised allele, 0.57kb band) in skeletal muscles (tibialis anterior, TA; soleus, SOL; diaphragm, DIA), but not in heart or liver from mKO mice (*Bmal1*^{f/f}; *Mlc1f-Cre*^{+/+}). (C) Loss of BMAL1 protein in skeletal muscle (gastrocnemius) from *Bmal1* mKO mouse demonstrated by Western blotting with anti-BMAL1 antibody. (D) Diurnal expression profile of *Bmal1* in TA and SOL muscles, and in heart (ventricles) from muscle-specific *Bmal1* mKO mice and control littermates (Ctrl). Transcripts were detected by qPCR and plotted relative to 36B4 expression (mean±SEM; arbitrary units; n=3/group/timepoint). Mice were sacrificed and tissues collected every 4 hours for 24 hours. ZT0=lights on, ZT12=lights off; dark phase shown by shaded area. (E) Generation of inducible muscle-specific *Bmal1* knockout (imKO) mice. The floxed *Bmal1* allele is deleted upon tamoxifen-mediated activation of the chimeric Cre recombinase, which is fused to a mutated estrogen receptor (ER) and controlled by the human α-skeletal actin promoter. (F) PCR products amplified from mouse DNA demonstrating disruption of *Bmal1* in skeletal muscle (TA), but not in heart following tamoxifen treatment. (G) Mean temporal expression of *Bmal1* and *Dbp* detected by qPCR and plotted relative to 36B4 expression (mean±SEM; arbitrary units; n=3-5/group/timepoint) in TA muscles from imKO mice and control littermates (Ctrl) 1 month after tamoxifen treatment. (H) Loss of BMAL1 protein in skeletal muscle demonstrated by western blotting with anti-BMAL1 antibody.

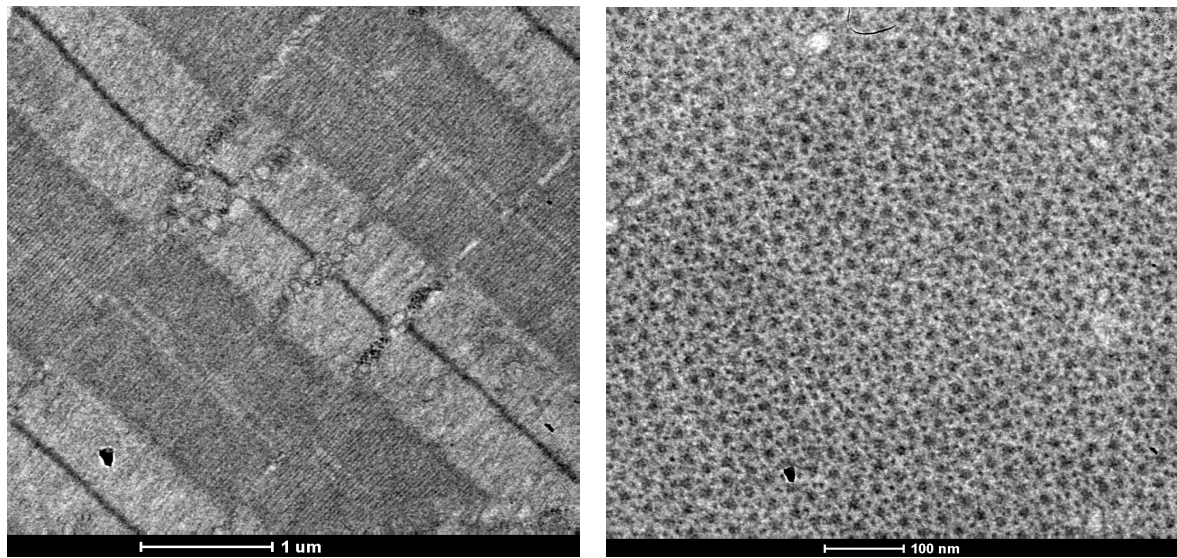


Figure S2 Electron microscopy of gastrocnemius from 6 month old mKO mouse showing normal sarcomere ultrastructure in both longitudinal (left panel) and transversal section (right panel).

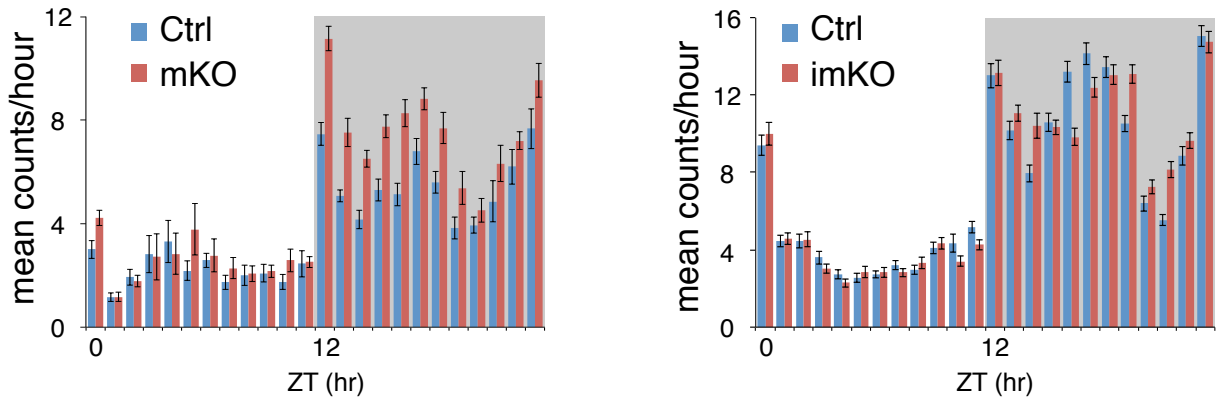


Figure S3 Circadian locomotor activity monitored by telemetry

Mean hourly locomotor activity counts from mKO mice and control littermates (left panel) and imKO mice and control littermates 1 month after tamoxifen (right panel) compared to controls (mean±SEM; n=3-5 mice/group). Mice were monitored continuously for 12 days.

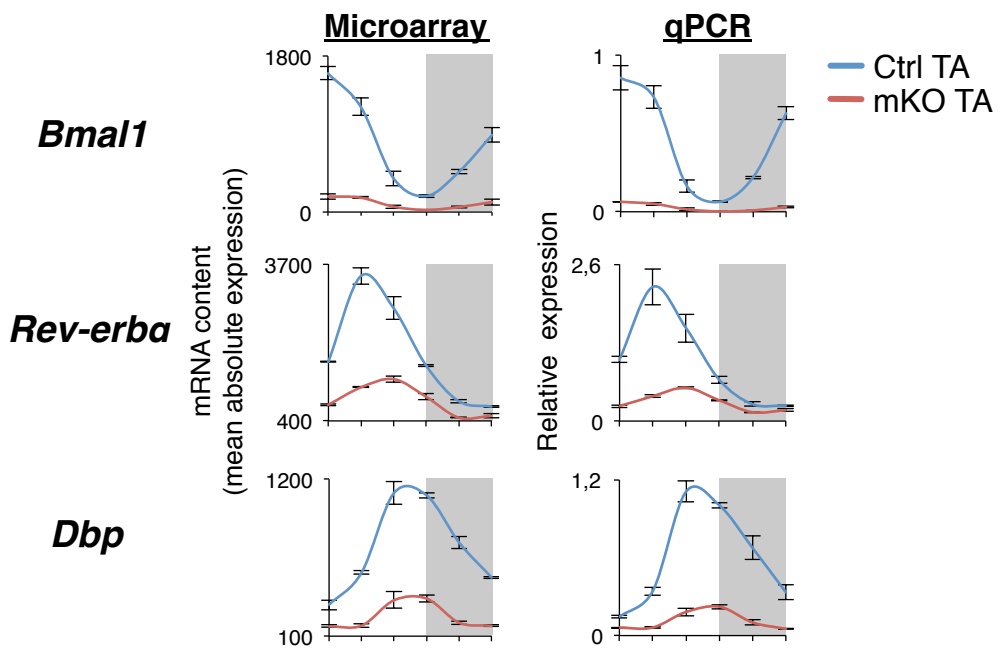


Figure S4 qPCR validation of selected genes

Microarray analysis of selected genes (mean \pm SEM; n=3/group/timepoint), was validated by qPCR and plotted relative to 36B4 expression (mean \pm SEM; arbitrary units; n=3/group/timepoint) in TA muscles. *Bmal1* microarray expression level was calculated summarizing only those oligonucleotide probes which hybridize to the exon coding for the *Bmal1* DNA binding domain, which is excised in mKO muscles.

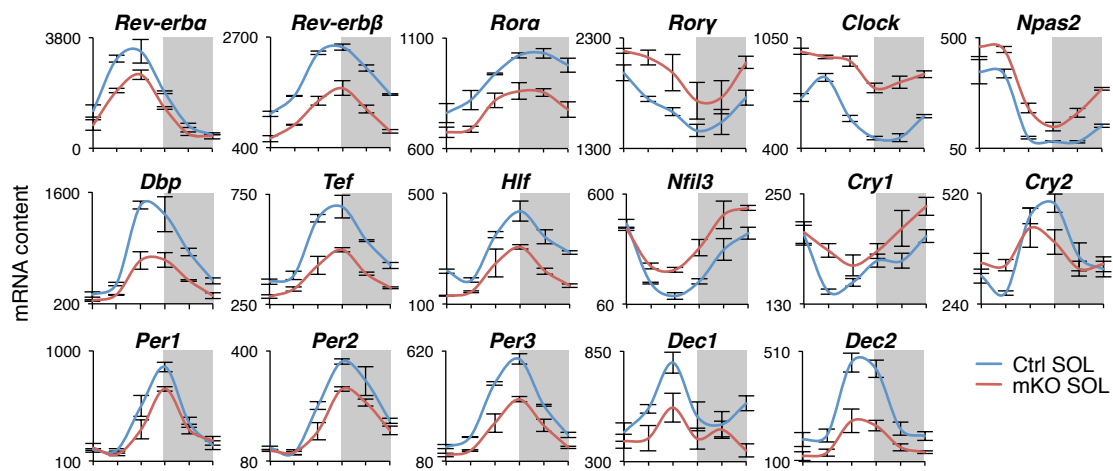


Figure S5 Circadian expression of core clock and clock-associated genes in soleus (SOL) muscles from control and mKO mice determined by microarray analysis and plotted as mean absolute expression levels (mean \pm SEM; n=3/group/timepoint).

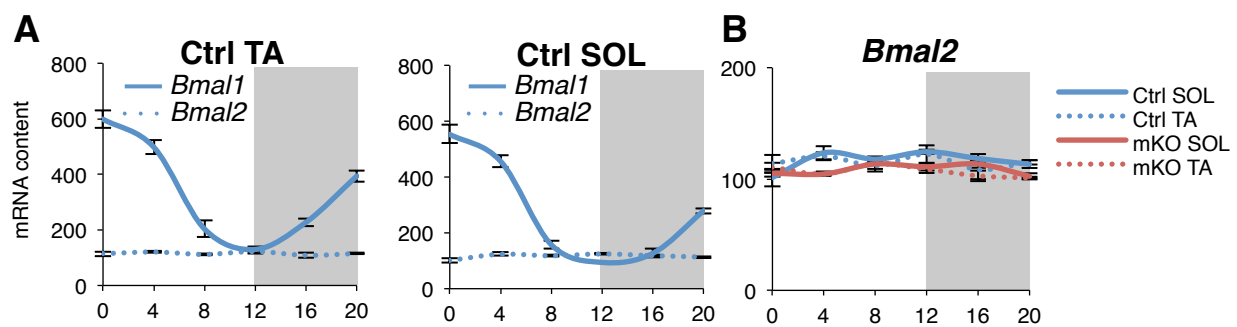


Figure S6 (A) Circadian expression of *Bmal2* (*Arntl2*) in TA and SOL muscles from control (Ctrl) mice determined by microarray analysis and plotted as mean absolute expression levels (mean \pm SEM; n=3/group/timepoint). **(B)** Comparison of *Bmal2* expression in Ctrl and mKO TA and SOL determined by microarray analysis (mean \pm SEM; n=3/group/timepoint).

B**Soleus**

Ctrl mKO

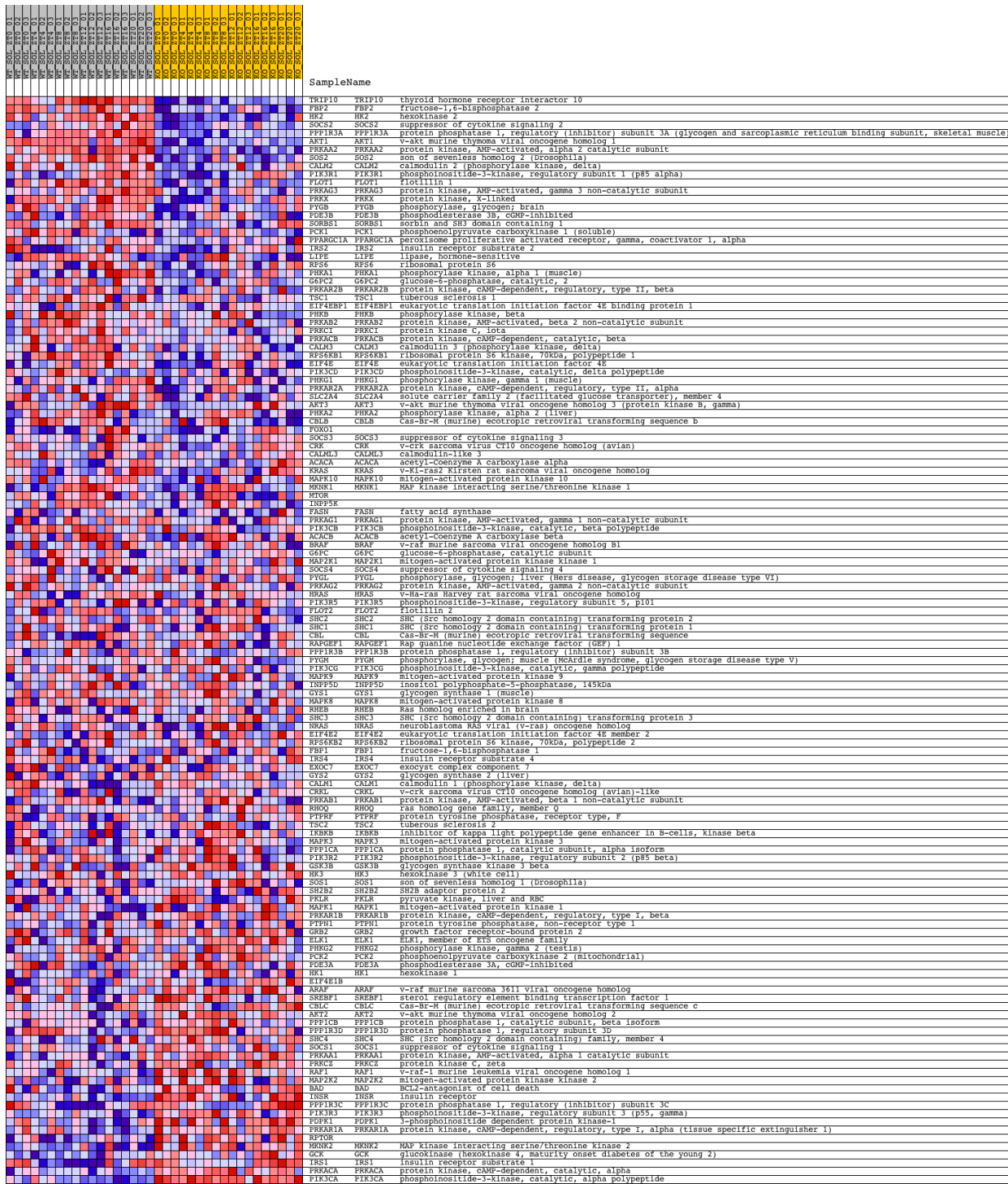


Figure S7B Same as Fig. S7A, but for SOL muscles.

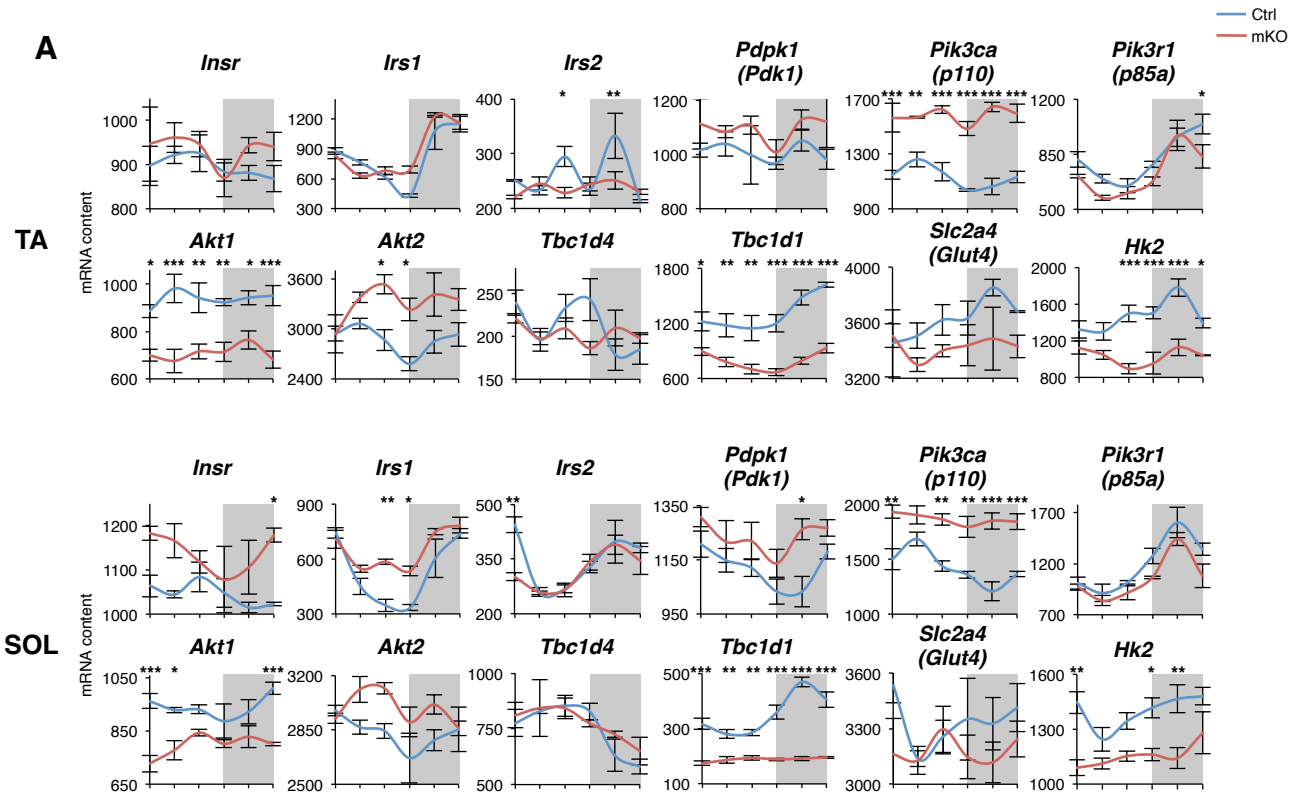


Figure S8 Diurnal gene expression profiles of insulin signaling mediators in TA and SOL muscles from control and mKO mice determined by microarray analysis and plotted as mean absolute expression levels (mean \pm SEM; n=3/group/timepoint; *p<0.05, **p<0.01, ***p<0.001, 2-way ANOVA with Bonferroni correction).

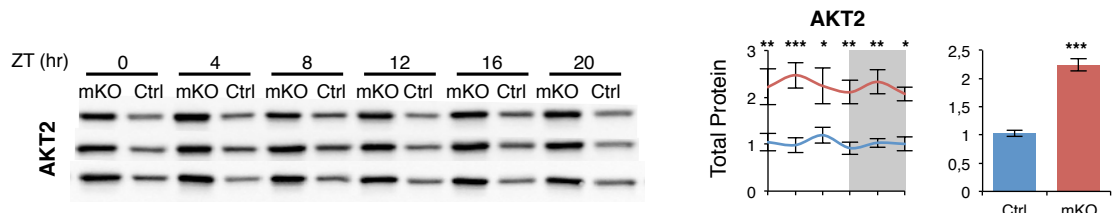
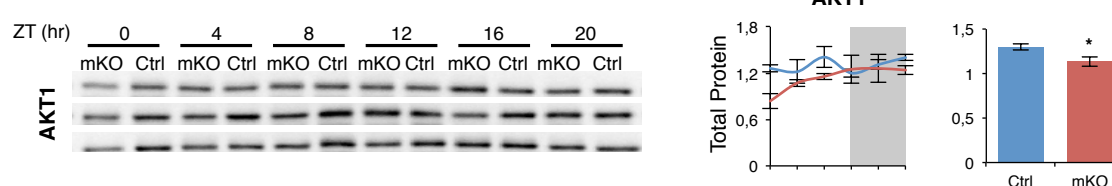
A**B**

Figure S9 (A,B) Western blots showing 24-hr protein levels of AKT2 (**A**) and AKT1 (**B**) in mKO and Ctrl gastrocnemius muscles from 36 different mice (n=3/group/timepoint). Middle panels show diurnal protein levels quantified by densitometry after western blot analysis (mean \pm SEM; arbitrary units; n=3/group/timepoint; *p<0.05, **p<0.01, ***p<0.001, 2-way ANOVA with Bonferroni correction, AKT2 group effect F=80.8, p<0.0001; AKT1 group effect F=7.14, p<0.05). Right panels show mean 24-hr protein levels (mean \pm SEM; arbitrary units; n=18/group; *p<0.05, ***p<0.0001, Student's t-test).

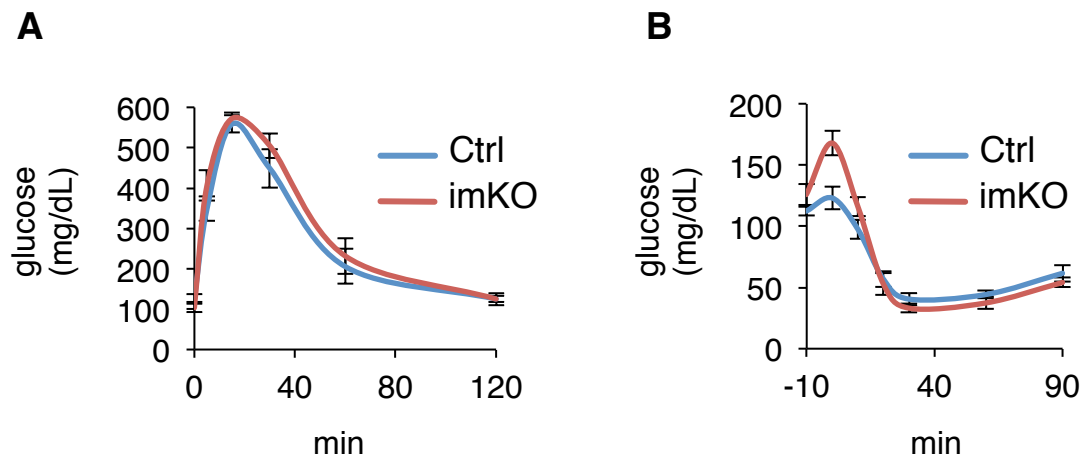


Figure S10 (A) Glucose tolerance test performed in imKO mice and control littermates (mean \pm SEM; n=5-6/group). **(B)** Insulin tolerance test performed in imKO mice and control littermates (mean \pm SEM; n=6/group).

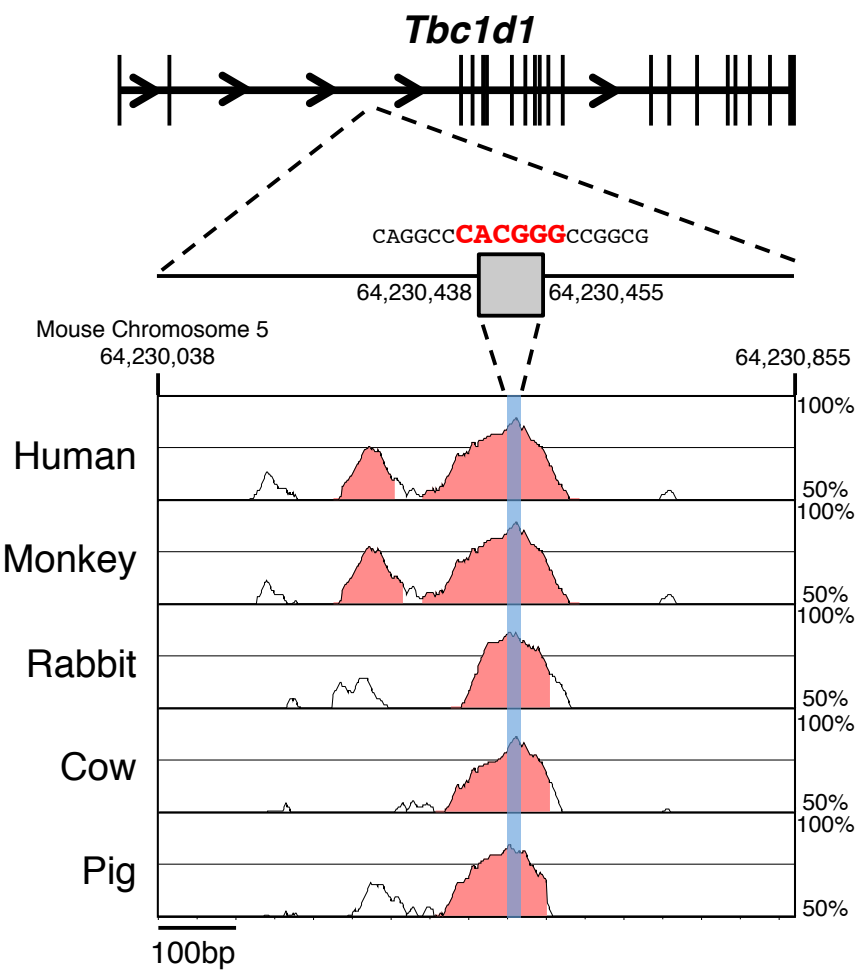


Figure S11 Graphical representation showing the location of the putative CLOCK:BMAL1 binding site in relation to the *Tbc1d1* gene, and the output of the VISTA analysis of the -400bp to +400bp region flanking the binding motif generated by comparing the mouse sequence (base genome) to that of 5 different mammalian species. Pink peaks represent conserved non-coding sequences. The position on mouse Chromosome 5 is given above the graph; numbers on the right indicate the percentage of conservation.

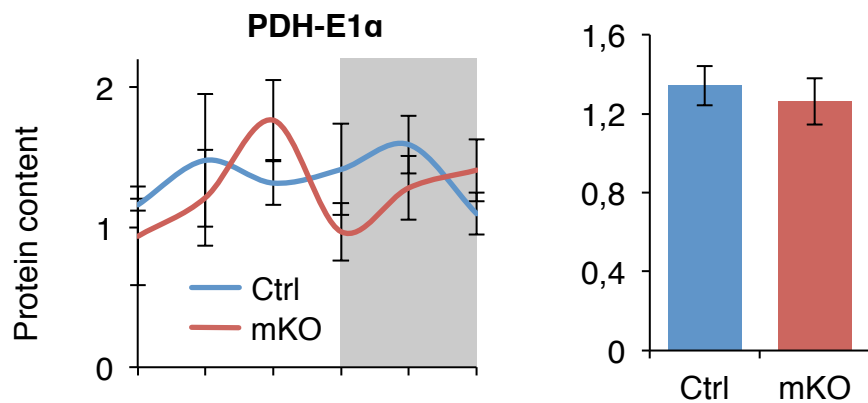


Figure S12 Diurnal protein levels of PDH-E1 α in gastrocnemius from Ctrl and mKO mice quantified by densitometry of Western blot (n=3/group/timepoint; mean \pm SEM; arbitrary units). Right panel shows mean PDH-E1 α for all timepoints in mKO and control (arbitrary units; mean \pm SEM; n=18/group)

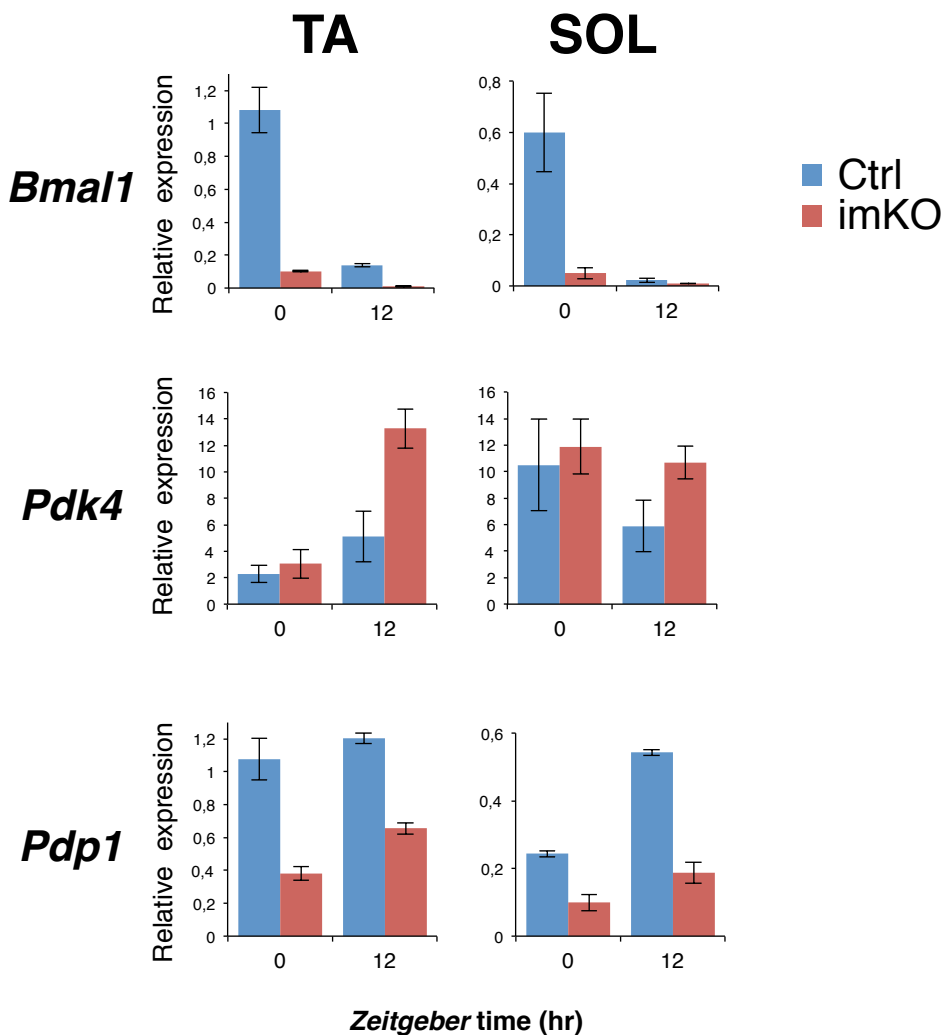


Figure S13 Long-term ablation of *Bmal1* in inducible mKO line

Gene expression in TA and SOL muscles from inducible muscle-specific *Bmal1* mKO mice (imKO) and control littermates (Ctrl). Mice were treated with tamoxifen (i.p. 1mg/day for 5 days) at 2 months of age, and sacrificed 5-months later at ZT0 and ZT12. Transcripts were detected by qPCR and plotted relative to *36B4* expression (mean±SEM; arbitrary units; n=3-4/group/timepoint).

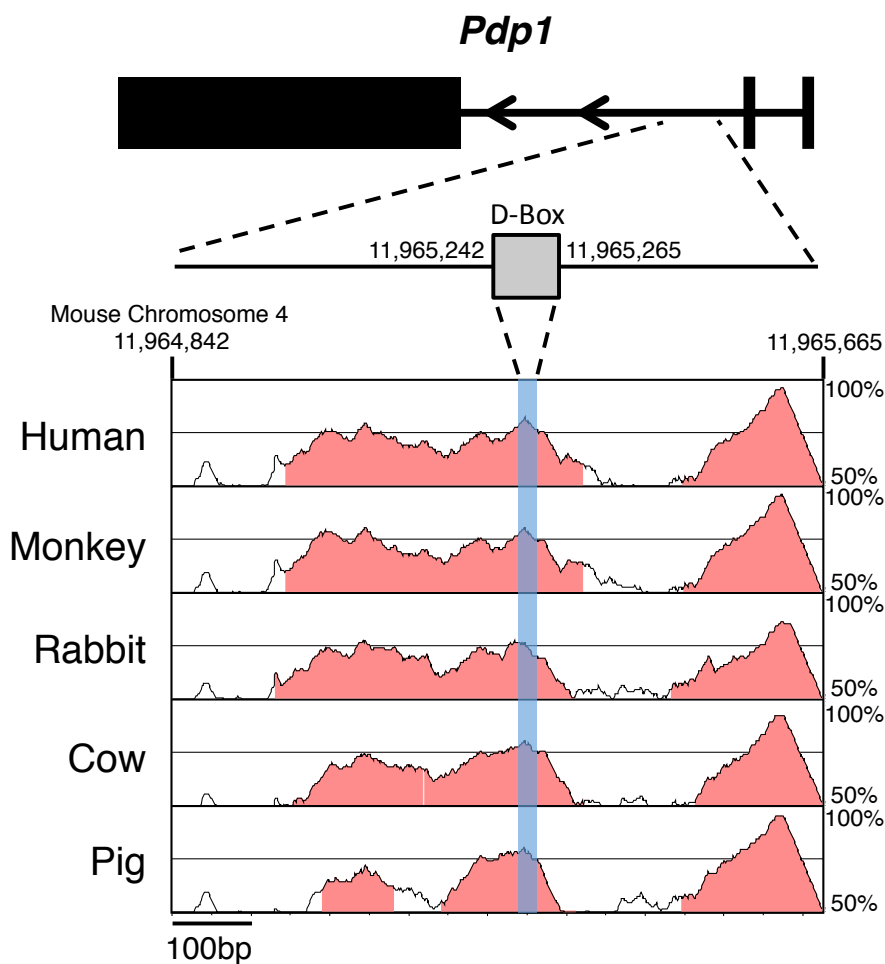


Figure S14 Graphical representation showing the location of the putative D-Box binding site in relation to the *Pdp1* gene, and the output of the VISTA analysis of the -400bp to +400bp region flanking the binding motif generated by comparing the mouse sequence (base genome) to that of 5 different mammalian species. Pink peaks represent conserved non-coding sequences. The position on mouse Chromosome 4 is given above the graph; numbers on the right indicate the percentage of conservation.

Table S1. Circadian metabolomic profiling of tibialis anterior muscle: changes in carbohydrate metabolism due to muscle-specific *Bmal1* knockout

Heat map of statistically significant metabolites profiled in this study. Paired comparisons (mKO vs Ctrl, n=5) at six time points during the day/night cycle (ZT0: lights on; ZT12: lights off). Shaded cells indicate $p \leq 0.05$ (red indicates that the mean values are significantly higher for that comparison; green indicates significantly lower; blue cells indicate $0.05 < p < 0.10$).

SUPER PATHWAY	SUB PATHWAY	BIOCHEMICAL NAME	HMDB	ANOVA Contrasts (Fold Change)					
				mKO - ZT0 CTRL - ZT0	mKO - ZT4 CTRL - ZT4	mKO - ZT8 CTRL - ZT8	mKO - ZT12 CTRL - ZT12	mKO - ZT16 CTRL - ZT16	mKO - ZT20 CTRL - ZT20
Carbohydrate	Aminosugars metabolism	erythronate	HMDB00613	0.80	0.81	0.54	0.76	1.66	0.88
		fucose	HMDB00174	1.07	0.97	0.55	0.57	1.07	1.27
	Fructose, mannose, galactose, starch, and sucrose metabolism	fructose	HMDB00660	1.69	1.77	0.76	1.04	1.14	1.13
		galactitol	HMDB00107	1.50	1.08	1.00	1.42	1.73	1.42
		6'-sialyllactose	HMDB06569	1.52	1.24	1.49	1.32	1.49	1.61
		maltose	HMDB00163	1.16	0.74	0.69	0.97	0.71	0.96
		mannitol	HMDB00765	1.22	0.93	0.85	1.21	1.51	1.27
		mannose	HMDB00169	2.09	2.00	0.99	0.86	1.12	0.96
		mannose-6-phosphate	HMDB01078	1.80	4.35	1.21	0.17	0.88	0.57
		sorbitol	HMDB00247	1.29	1.38	1.00	1.16	1.59	1.77
		maltooltriose	HMDB01262	1.47	0.78	0.73	1.14	0.54	0.81
		malotetraose	HMDB01296	1.77	1.13	0.88	1.01	0.63	1.18
	Glycolysis, gluconeogenesis, pyruvate metabolism	1,5-anhydroglucitol (1,5-AG)	HMDB02712	1.00	0.97	0.85	0.97	1.09	1.21
		glycerate	HMDB00139	0.90	0.79	1.21	0.91	1.01	0.74
		glucose-6-phosphate (G6P)	HMDB01401	1.92	4.43	1.29	0.15	0.87	0.61
		glucose 1-phosphate	HMDB01586	1.74	1.69	0.79	1.03	0.92	1.28
		glucose	HMDB00122	1.37	1.04	0.92	1.14	1.03	1.03
		1,6-anhydroglucose	HMDB00640	1.35	0.97	1.09	0.93	0.78	1.22
		fructose-6-phosphate	HMDB00124	1.88	3.44	1.17	0.24	0.83	0.72
		fructose 1-phosphate	HMDB01076	1.53	1.01	0.98	1.13	1.05	0.88
		Isobar: fructose 1,6-diphosphate, glucose 1,6-diphosphate, myo-inositol 1,4 or 1,3-diphosphate		1.53	0.97	1.21	1.01	1.03	0.84
		2-phosphoglycerate	HMDB03391	0.86	0.73	1.21	0.78	1.01	0.75
	Nucleotide sugars, pentose metabolism	3-phosphoglycerate	HMDB00807	0.91	0.73	1.07	0.78	1.13	0.73
		dihydroxyacetone phosphate (DHAP)	HMDB01473	1.04	1.27	1.56	2.20	2.11	0.80
		phosphoenolpyruvate (PEP)	HMDB00263	0.97	0.70	1.18	0.97	1.19	0.79
		pyruvate	HMDB00243	0.85	0.93	1.10	0.72	1.02	0.79
		lactate	HMDB00190	0.95	0.90	0.93	0.95	1.14	0.97
		arabitol	HMDB01851	1.71	0.87	0.99	1.15	1.65	1.43
		ribitol	HMDB00508	1.29	1.36	1.41	1.42	1.60	1.39
	Nucleotide sugars, pentose metabolism	ribose	HMDB00283	1.26	1.01	1.20	1.07	1.38	1.01
		ribose 5-phosphate	HMDB00618	0.93	0.90	1.21	0.71	1.61	0.63
		ribulose	HMDB00621	1.29	1.00	1.29	1.16	1.33	0.88
		Isobar: ribulose 5-phosphate, xylulose 5-phosphate		0.99	0.98	1.03	0.87	1.35	0.83
	Nucleotide sugars, pentose metabolism	xylitol	HMDB00568	4.19	1.00	0.95	1.55	2.84	1.56
		xylulose	HMDB00654	1.38	1.21	1.27	1.18	1.59	1.12